Neural Network-Based Control and Active Vibration Mitigation in a Fully-Flexible Arm Space Robot under Elastic Base Influence: A Luenberger Observer Approach

Lijiao Zhang[1], Xiaoyan Yu[2]*

[1] Mechanical and Electrical Engineering Practice Center, Fuzhou University, 350108 Fuzhou, China
[2] School of Mechanical Engineering and Automation, Fuzhou University, 350108 Fuzhou, China

* Correspondence: Xiaoyan Yu (cool@fzu.edu.cn)

Citation: L. J. Zhang and X. Y. Yu, "Neural network-based control and active vibration mitigation in a fully-flexible arm space robot under elastic base influence: A luenberger observer approach," *J. Intell Syst. Control*, vol. 2, no. 4, pp. 197–208, 2023. https://doi.org/10.56578/jisc020402.

Abstract: This study explores dynamic simulation and integrated control in a space robotic arm system characterized by a fully-flexible arm and an elastic base. The elastic base is modeled as a lightweight spring, and the modal shapes of a simply-supported beam are selected via the assumed mode method to represent the bending vibrations of the flexible arm. Dynamic equations for the system are formulated by integrating Lagrangian mechanics with momentum conservation principles. The approach involves reducing the system into two lower-order subsystems using a dual-time-scale singular perturbation method. The first subsystem, exhibiting slow variation, accounts for the joint's rigid motion, while the second, fast-varying subsystem addresses the vibrations of the base and arm. Estimation of joint velocities is conducted through a Luenberger observer, complemented by the use of an Radial Basis Function (RBF) neural network to approximate parameter uncertainties within the system. This facilitates the control of rigid motion in the slow-varying subsystem. Subsequently, the fast-varying subsystem's vibration is actively controlled based on linear system optimal control theory. Numerical simulations validate the integrated control approach's effectiveness in managing both motion and vibration, demonstrating its potential in enhancing the operational precision and stability of space robot systems.

Keywords: Space robot; Fully-flexible arm; Elastic base; Active vibration mitigation; Neural network; Luenberger observer

1 Introduction

The field of space robotic arms has significantly advanced the application of novel space technologies, capturing the attention of the global research community [1–5]. Operating in the unique challenges of space, characterized by high vacuum, microgravity, substantial temperature fluctuations, intense radiation, and dim illumination, space robotic arm systems differ markedly from their terrestrial counterparts [6, 7]. The inherent nonlinearity and strong coupling in space robotic arms preclude the straightforward application of control methods used for terrestrial robots. A substantial body of research has thus focused on the dynamics and control of space robotic arms under varied operational conditions [8–12]. For instance, Huang and Chen [10] have explored kinematic control of rigid space robotic arms using bidirectional mapping neural networks, developing a method for convergent inverse kinematics control. Zhang and Chen [11] have tackled trajectory tracking and vibration suppression in space robotic arm systems with mixed rigid-flexible arms, proposing an adaptive fuzzy $H\infty$ control algorithm for systems encountering external disturbances. Further, Jing and Li [12] have investigated the effects of collisions and subsequent stable control in dual-arm space robot systems during satellite capture operations.

In light of the need to economize on expensive launch energy and prolong the lifespan of orbital missions, the weight of space robotic arms is a critical consideration. Characteristically featuring long arms and substantial loads, these arms exhibit notable flexibility. This flexibility demands thorough consideration due to its substantial impact on the overall system. Presently, a diverse range of research and practical applications are directed at terrestrial robotic arm systems with flexible components [13, 14]. Halalchi et al. [13] addressed the challenges in modeling and controlling flexible-link robots using Linear Parameter-Varying (LPV) approaches. Additionally, Shawky et

al. [14] devised a controller for space robotic arms with limited output torque, achieving joint trajectory tracking while concurrently suppressing flexibility-induced vibrations.

The dynamics and control mechanisms of multi-flexible arm space robotic arm systems present greater complexity compared to their terrestrial counterparts. A critical challenge in these systems is the rapid attenuation of vibrations induced by the flexible arms once joint positioning is accomplished. Consequently, the investigation into the dynamic characteristics of flexible arms and the formulation of effective control strategies are essential in the realm of space robotic arm research and applications [15, 16]. Additionally, the mounting of space robotic arms on mobile truss rails, while expanding operational range, invariably leads to vibration within these rails. Primarily, these vibrations stem from the robust coupling between the space robotic arm and its carrier, as well as the movement of the large-mass arm along the rails. In the unique damping-free environment of outer space, mitigating these rail vibrations poses a significant challenge [17–19].

In light of these discussions, there is a pressing need to delve into the dynamics and control challenges of fully-flexible arm space robotic arm systems influenced by base elasticity. This research simplifies the rail elasticity of the space robotic arm to a lightweight spring for initial analysis. The assumed mode method is strategically employed to select the modal shapes of a simply-supported beam, representing the bending vibration modes of the flexible arm. The dynamic equations for a dual flexible-rod space robotic arm system, influenced by base elasticity, are then formulated, incorporating the system's positional geometric relations, conservation of momentum principles, and Lagrangian equations. To achieve integrated control over the joint motion and vibration of the space robotic arm system, a dual-time-scale singular perturbation method is utilized. This method effectively reduces the system into two lower-order subsystems: the first, a slow-varying subsystem, encapsulates the joint's rigid motion, and the second, a fast-varying subsystem, addresses the base and arm vibrations. Joint velocities are estimated using a Luenberger observer, complemented by an RBF neural network which approximates uncertainties in system parameters, thus facilitating control over the rigid motion of the slow-varying subsystem. Active vibration control in the fast-varying subsystem is subsequently implemented based on linear system optimal control theory. Numerical simulations validate the efficacy of the proposed controllers in managing joint motion, arm vibration, and base vibration.

2 System Dynamics Modeling

This section elucidates the dynamic modeling of a fully-flexible arm space robot system, operating under the influence of a planar motion elastic base, as delineated in Figure 1. An inertial coordinate system, designated as $O - XY$, is established, choosing an arbitrary point O in space as the origin. This system encompasses an elastic base, referred to as B_0, and a flexible arm rod, labeled $B_i (i = 1, 2, \cdots, n)$. The latter is conceptualized as an Euler-Bernoulli cantilever beam, exclusively generating transverse vibrations. The components B_{i-1} and B_i are interconnected via rigid joints, marked as $O_i (i = 1, 2, \cdots, n)$.

For simplification in this study, the elasticity of the base, symbolized by the rail, is modeled as a spring with a constant stiffness coefficient. In the context of the substantial mass of both the space robot and its base relative to the rail, their weight is deemed negligible. According to vibration theory, the primary direction of vibration is perpendicular to the rail. In this simplified model, a lightweight spring connects the rotational hinge, denoted as O_1, with the elastic base, identified as B_0. This spring substitutes for the elastic vibration of the base, under the assumptions that: a) the spring is massless; b) it undergoes only extension and compression movements; c) its elasticity coefficient, labeled $\boldsymbol{K}_x$, remains constant. Additionally, $\boldsymbol{x}'$ signifies the elastic displacement of the base.

Inertial coordinate systems, marked as $O - XY$, along with the principal axis body coordinate systems for each subsystem B_i, identified as $O_i - x_i y_i$, are instituted. The symbol C represents the total center of mass of the system. The flexible arm rod, tagged as B_i, possesses a uniform mass density per unit length, annotated as ρ_i, and a uniform bending stiffness, marked as EI_i.

The bending vibration modes of the flexible arm, referred to as $B_i (i = 1, 2, \cdots, n)$, are ascertained using the assumed mode method. The transverse elastic deformation $w_i(X_i, t)$ of the flexible arm rod B_i at the longitudinal coordinate $X_i (0 < X_i < l_i)$ and at time t is expressed as:

$$w_i(x_i, t) = \sum_{j=1}^{n_i} \varphi_{ij}(x_i) \delta_{ij}(t) \tag{1}$$

where, $\varphi_{ij}(X_i)$ symbolizes the j-th order mode function of the flexible arm $B_i (i = 1, 2, \cdots, n)$, with $\varphi_{ij}(X_i) = \sin(j\pi X_i/l_i)$, denoting the selection of simply-supported beam modal functions for computing the coefficients and free terms of elastic deformation in the fully-flexible arm space robot system. The cutoff order is n_i, with $\delta_{ij}(t)$ signifying the vibrational modal coordinates of $\varphi_{ij}(X_i)$. Considering that lower-order modes exert a dominant influence on the vibration of the flexible arm rod, higher-order modal terms in Eq. (1) are omitted, focusing on the initial two lower-order modes, i.e., $n_i = 2 (i = 1, 2, \cdots, n)$.
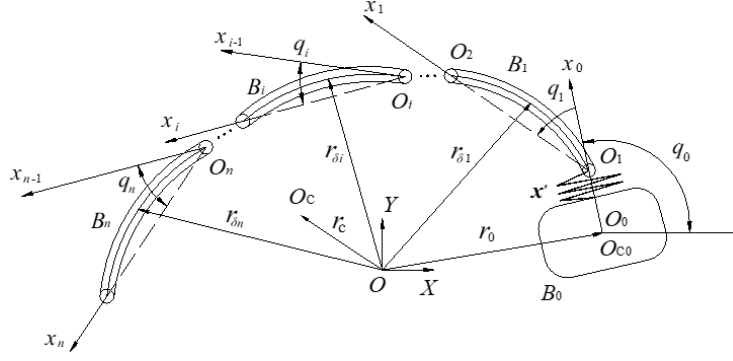
Figure 1. Space robot with elastic base and flexible arms

2.1 Kinematic Fundamental Equations

The derivation of the kinematic fundamental equations for a fully-flexible arm space robot system, influenced by an elastic base as depicted in Figure 1, proceeds as follows. Drawing on the findings from references [20–22] and the model presented in Figure 1, the vector of any point on each flexible arm rod of the space robot system, relative to the origin O of the inertial coordinate system O-XY, is articulated. This vector, denoted as $\boldsymbol{r}_{\delta i}(i = \mathrm{r}+1, \mathrm{r}+2, \cdots, n)$ is expressed in Eq. (2):

$$\boldsymbol{r}_{\delta i} = \boldsymbol{r}_0 + x'\boldsymbol{e}_{x0} + \sum_{j=0}^{i-1} l_j \boldsymbol{e}_{xj} + X_i \boldsymbol{e}_{xi} + w_i\left(X_i, t\right)\boldsymbol{e}_{yi} \tag{2}$$

where, $\boldsymbol{e}_{xj} = \left[\cos\left(\sum_{k=0}^{j} q_k\right), \sin\left(\sum_{k=0}^{j} q_k\right)\right]^{\mathrm{T}}, \boldsymbol{e}_{yj} = \left[-\sin\left(\sum_{k=0}^{j} q_k\right), \cos\left(\sum_{k=0}^{j} q_k\right)\right]^{\mathrm{T}} (j = 0, 1, 2, \cdots, i)$.

The derivation continues by differentiating Eq. (2) with respect to time , yielding the velocity vector of any point on each flexible arm rod relative to the origin O of the inertial system O-XY. This velocity vector, represented as $\dot{\boldsymbol{r}}_{\delta i}(i = \mathrm{r}+1, \mathrm{r}+2, \cdots, n)$, is captured in Eq. (3):

$$\dot{\boldsymbol{r}}_{\delta i} = \dot{\boldsymbol{r}}_0 + x'\dot{\boldsymbol{e}}_{x0} + \sum_{j=0}^{i-1} l_j \dot{\boldsymbol{e}}_{xj} + X_i \dot{\boldsymbol{e}}_{xi} + w_i\left(X_i, t\right)\dot{\boldsymbol{e}}_{\mathrm{yi}} + \dot{w}_i\left(X_i, t\right)\boldsymbol{e}_{yi} \tag{3}$$

where, $\dot{\boldsymbol{e}}_{xj} = \left(\sum_{k=0}^{j} \dot{q}_k\right)\left[-\sin\left(\sum_{k=0}^{j} q_k\right), \cos\left(\sum_{k=0}^{j} q_k\right)\right]^{\mathrm{T}}, \dot{\boldsymbol{e}}_{yj} = \left(\sum_{k=0}^{j} \dot{q}_k\right)\left[-\cos\left(\sum_{k=0}^{j} q_k\right), -\sin\left(\sum_{k=0}^{j} q_k\right)\right]^{\mathrm{T}} (j = 0, 1, 2, \cdots, i)$.

In the context of outer space, where the system exists in a state of weightlessness, the fully-flexible arm space robot system under the influence of an elastic base adheres to a conservation of momentum relationship relative to the inertial coordinate system O-XY. This relationship is encapsulated in Eq. (4):

$$m_0 \dot{\boldsymbol{r}}_0 + \sum_{i=1}^{n}\left(\rho_i \int_0^{l_i} \dot{\boldsymbol{r}}_{\delta i}\,\mathrm{d}X_i\right) = M\dot{\boldsymbol{r}}_{\mathrm{C}} \tag{4}$$

Substituting Eq. (3) into Eq. (4), the resultant expression is provided in Eq. (5):

$$\dot{\boldsymbol{r}}_0 = \dot{\boldsymbol{r}}_{\mathrm{C}} + \sum_{j=0}^{n} L_{xj}\dot{\boldsymbol{e}}_{xj} + \sum_{j=\mathrm{r}+1}^{n}\left(\sum_{k=1}^{n_i} L_{yjk}\delta_{jk}\right)\dot{\boldsymbol{e}}_{yj} + \sum_{j=\mathrm{r}+1}^{n}\left(\sum_{k=1}^{n_i} L_{yjk}\dot{\delta}_{jkk}\right)\boldsymbol{e}_{yj} \tag{5}$$

where, L_{xj} and L_{yjk} are identified as combined functions of the system's inertial parameters.

Further substitution of Eq. (5) into Eq. (3) leads to the derivation of Eq. (6).

$$\begin{aligned}
\dot{\boldsymbol{r}}_{\delta i} =&\,\dot{\boldsymbol{r}}_{\mathrm{C}} + \sum_{j=0}^{n} L_{xj}\dot{\boldsymbol{e}}_{xj} + \sum_{j=\mathrm{r}+1}^{n}\left(\sum_{k=1}^{n_i} L_{yjk}\delta_{jk}\right)\dot{\boldsymbol{e}}_{yj} + \sum_{j=\mathrm{r}+1}^{n}\left(\sum_{k=1}^{n_i} L_{yjk}\dot{\delta}_{jkk}\right)\boldsymbol{e}_{yj} + x'\dot{\boldsymbol{e}}_{x0} \\
&+ \sum_{j=0}^{i-1} l_j \dot{\boldsymbol{e}}_{xj} + X_i \dot{\boldsymbol{e}}_{xi} + w_i\left(X_i, t\right)\dot{\boldsymbol{e}}_{\mathrm{yi}} + \dot{w}_i\left(X_i, t\right)\boldsymbol{e}_{\mathrm{yi}}
\end{aligned} \tag{6}$$

2.2 Fundamental Dynamics Equations

Expanding upon the kinematic fundamental equations delineated in section 2.1 for the fully-flexible arm space robot system under the influence of an elastic base, the fundamental dynamics equations are derived here by integrating the principles of Lagrangian mechanics. As illustrated in Figure 1, the kinetic energy, represented as T_0, of the elastic base within the fully-flexible arm space robot system is formulated in Eq. (7):

$$T_0 = \frac{1}{2} \left(m_0 \dot{\boldsymbol{r}}_0 + J_0 \dot{q}_0^2 \right) \tag{7}$$

The kinetic energy of each flexible arm rod, denoted as $T_{\delta i}(i = 1, 2, \cdots, n)$, is articulated in Eq. (8):

$$T_{\delta i} = \frac{1}{2} \rho_i \int_0^{l_i} \dot{r}_{\delta i}^2 dX_i \tag{8}$$

Consequently, the total kinetic energy of the system, expressed as T, is encapsulated in Eq. (9):

$$T = T_0 + \sum_{i=\mathrm{r}+1}^{n} T_{\delta i} \tag{9}$$

In the unique weightless environment of outer space, the total potential energy of the system, labeled as U, emanates from the combined bending strain energy of the flexible arms and the elastic potential energy of the elastic base, as defined in Eq. (10):

$$U = \frac{1}{2} \sum_{i=1}^{n} \left((EI)_i \int_0^{l_i} \left(\frac{\partial^2 w_i \left(X_i, t \right)}{\partial^2 X_i} \right)^2 \mathrm{d}X_i \right) + \frac{1}{2} \boldsymbol{K}_x \boldsymbol{x}'^2 \tag{10}$$

The system's rigid generalized coordinates are defined as $\boldsymbol{\theta}_{\mathrm{r}} = [q_0, q_1, q_2, \cdots, q_{\mathrm{r}}]^{\mathrm{T}} \in R^{(\mathrm{r}+1) \times 1}$, while the flexible arm rod's generalized coordinates are denoted as $\boldsymbol{\theta}_{\delta} = [\delta_{11}, \cdots, \delta_{1n_1}, \delta_{21} \cdots, \delta_{2m_1}, \cdots, \delta_{m_n}]^{\mathrm{T}} \in R^{\left(\sum_{i=+1}^{\mathrm{n}} n_i \right) \times 1}$, with $\boldsymbol{\theta} = \left[\boldsymbol{\theta}_{\mathrm{r}}^{\mathrm{T}}, \boldsymbol{\theta}_{\delta}^{\mathrm{T}}, \boldsymbol{x}' \right]^{\mathrm{T}} \in R^{\left(\mathrm{r}+2+\sum_{i=+1}^{\mathrm{n}} n_i \right) \times 1}$. Employing the second kind of Lagrange's equations $L = T - U$, the fundamental dynamics equation of the system with uncontrolled base position but controlled attitude is derived, incorporating the total kinetic energy Eq. (9) and total potential energy Eq. (10):

$$\boldsymbol{D}(\boldsymbol{\theta}) \begin{bmatrix} \ddot{\boldsymbol{\theta}}_{\mathrm{r}} \\ \ddot{\boldsymbol{\theta}}_{\delta} \\ \ddot{\boldsymbol{x}}' \end{bmatrix} + \boldsymbol{H}(\boldsymbol{\theta}, \dot{\boldsymbol{\theta}}) \begin{bmatrix} \dot{\boldsymbol{\theta}}_{\mathrm{r}} \\ \dot{\boldsymbol{\theta}}_{\delta} \\ \dot{\boldsymbol{x}}' \end{bmatrix} + \begin{bmatrix} \boldsymbol{0}_{(n+1) \times 1} \\ \boldsymbol{K}_{\delta} \boldsymbol{\theta}_{\delta} \\ \boldsymbol{K}_x \boldsymbol{x}' \end{bmatrix} = \begin{bmatrix} \boldsymbol{\tau} \\ \boldsymbol{0}_{n_i n \times 1} \\ \boldsymbol{0}_{1 \times 1} \end{bmatrix} \tag{11}$$

where, $D(\boldsymbol{\theta})$ represents the positive definite and symmetric inertia matrix pertaining to (n+2+n_in)×(n+2+ n_in). $C\left(\theta_{r\delta}, \dot{\theta}_{r\delta} \right)$ is the matrix vector that includes centrifugal and Coriolis forces of (n+1+n_in)×(n+1+n_in). $\tau = \left[\tau_0, \tau_{\mathrm{r}}^{\mathrm{T}} \right]^{\mathrm{T}} = [\tau_0, \tau_1, \tau_2, \cdots, \tau_n]^{\mathrm{T}}$ denotes the system's control input torque vector, and $\boldsymbol{K}_{\delta} = \mathrm{diag}\left[\boldsymbol{K}_{\delta 1}, \boldsymbol{K}_{\delta 2}, \cdots, \boldsymbol{K}_{\delta n} \right]$ and $\boldsymbol{K}_{\delta i} = \mathrm{diag}\left[k_{i1}, k_{i2}, \cdots, k_{in_i} \right]$ are the stiffness coefficient matrices of the flexible arm.

3 System Dynamics Singular Perturbation Modeling

In addressing the impact of vibrations induced by the elastic base and flexible arms during operational movements on both the accuracy of position control and overall system stability, a dual-time-scale singular perturbation model is developed. This model, founded on the concept of integral flow, serves to bifurcate the system dynamics model of the fully-flexible arm space robot system under elastic base influence into two distinct subsystems characterized by fast and slow variations.

From the dynamic model as delineated in Eq. (11), the system under the influence of an elastic base is elaborated upon. The model is expressed in Eq. (12).

$$\begin{bmatrix} \boldsymbol{D}_{11} & \boldsymbol{D}_{12} \\ \boldsymbol{D}_{21} & \boldsymbol{D}_{22} \end{bmatrix} \begin{bmatrix} \ddot{\boldsymbol{\theta}}_{\mathrm{r}} \\ \ddot{\boldsymbol{\theta}}_{\delta x} \end{bmatrix} + \begin{bmatrix} \boldsymbol{H}_{11} & \boldsymbol{H}_{12} \\ \boldsymbol{H}_{21} & \boldsymbol{H}_{22} \end{bmatrix} \begin{bmatrix} \dot{\boldsymbol{\theta}}_{\mathrm{r}} \\ \dot{\boldsymbol{\theta}}_{\delta x} \end{bmatrix} + \begin{bmatrix} \boldsymbol{\theta}_{(n+1) \times 1} \\ \boldsymbol{K}_{\delta x} \boldsymbol{\theta}_{\delta x} \end{bmatrix} = \begin{bmatrix} \boldsymbol{\tau} \\ \boldsymbol{0}_{(n_i n+1) \times 1} \end{bmatrix} \tag{12}$$

where, $\boldsymbol{\theta}_{\delta x} = \left[\boldsymbol{\theta}_{\delta}^{\mathrm{T}}, \boldsymbol{x}' \right]^{\mathrm{T}}$, and $\boldsymbol{K}_{\delta x} = \mathrm{diag}\left[\boldsymbol{K}_{\delta}, \boldsymbol{K}_x \right]$ is the composite stiffness matrix; $\boldsymbol{D}_{11} \in R^{(n+1) \times (n+1)}$, $\boldsymbol{D}_{12} \in R^{(n+1) \times (n_i n+1)}, \boldsymbol{D}_{21} \in R^{(n_i n+1) \times (n+1)}$, and $\boldsymbol{D}_{22} \in R^{(n_i n+1) \times (n_i n+1)}$ are the corresponding sub-matrices of $\boldsymbol{D}(\boldsymbol{\theta})$; similarly, $\boldsymbol{H}_{11} \in R^{(n+1) \times (n+1)}$, $\boldsymbol{H}_{12} \in R^{(n+1) \times (n_i n+1)}$, $\boldsymbol{H}_{21} \in R^{(n_i n+1) \times (n+1)}$, and $\boldsymbol{H}_{22} \in R^{(n_i n+1) \times (n_i n+1)}$ are respective sub-matrices of $\boldsymbol{H}(\boldsymbol{\theta}, \dot{\boldsymbol{\theta}})$. Given that $\boldsymbol{D}(\boldsymbol{\theta})$ is a symmetric and positive definite inertia matrix of the system, its inverse is formulated as $\boldsymbol{G}(\boldsymbol{\theta})$ in Eq. (13):

$$G(\boldsymbol{\theta}) = \left[\begin{array}{cc} \boldsymbol{G}_{11} & \boldsymbol{G}_{12} \\ \boldsymbol{G}_{21} & \boldsymbol{G}_{22} \end{array} \right] = \left[\begin{array}{cc} \boldsymbol{D}_{11} & \boldsymbol{D}_{12} \\ \boldsymbol{D}_{21} & \boldsymbol{D}_{22} \end{array} \right]^{-1} \tag{13}$$

where, $\boldsymbol{G}_{11} = \left(\boldsymbol{D}_{11} - \boldsymbol{D}_{12}\boldsymbol{D}_{22}^{-1}\boldsymbol{D}_{21} \right)^{-1}$, $\boldsymbol{G}_{22} = \left(\boldsymbol{D}_{22} - \boldsymbol{D}_{21}\boldsymbol{D}_{11}^{-1}\boldsymbol{D}_{12} \right)^{-1}$, $\boldsymbol{G}_{21} = -\boldsymbol{G}_{22}\boldsymbol{D}_{21}\boldsymbol{D}_{11}^{-1}$, $\boldsymbol{G}_{12} = -\boldsymbol{G}_{11}\boldsymbol{D}_{12}\boldsymbol{D}_{22}^{-1}$. Consequently, Eq. (12) undergoes a transformation, leading to the formulations in Eqs. (14) and (15):

$$\ddot{\boldsymbol{\theta}}_{\mathrm{r}} = \boldsymbol{G}_{11}\boldsymbol{\tau} - \boldsymbol{G}_{12}\boldsymbol{K}_{\delta x}\boldsymbol{\theta}_{\delta x} - \boldsymbol{G}_{11}\left[\boldsymbol{H}_{11}\dot{\boldsymbol{\theta}}_{\mathrm{r}} + \boldsymbol{H}_{12}\dot{\boldsymbol{\theta}}_{\delta x} \right] - \boldsymbol{G}_{12}\left[\boldsymbol{H}_{21}\dot{\boldsymbol{\theta}}_{\mathrm{r}} + \boldsymbol{H}_{22}\dot{\boldsymbol{\theta}}_{\delta x} \right] \tag{14}$$

$$\ddot{\boldsymbol{\theta}}_{\delta x} = \boldsymbol{G}_{21}\boldsymbol{\tau} - \boldsymbol{G}_{22}\boldsymbol{K}_{\delta x}\boldsymbol{\theta}_{\delta x} - \boldsymbol{G}_{21}\left[\boldsymbol{H}_{11}\dot{\boldsymbol{\theta}}_{\mathrm{r}} + \boldsymbol{H}_{12}\dot{\boldsymbol{\theta}}_{\delta x} \right] - \boldsymbol{G}_{22}\left[\boldsymbol{H}_{21}\dot{\boldsymbol{\theta}}_{\mathrm{r}} + \boldsymbol{H}_{22}\dot{\boldsymbol{\theta}}_{\delta x} \right] \tag{15}$$

With an assumption that the smallest stiffness in the composite stiffness matrix $\boldsymbol{K}_{\delta x}$ is $k_{\min}$, with $\mu^2 k_{\min} = 1$, a singular perturbation factor is defined as μ. Let $\mu^2\boldsymbol{\zeta}_{\delta x} = \boldsymbol{\theta}_{\delta x}$ and $\boldsymbol{K}_\mu = \mu^2\boldsymbol{K}_{\delta x}$, Eqs. (14) and (15) evolve into Eqs. (16) and (17):

$$\ddot{\boldsymbol{\theta}}_{\mathrm{r}} = \boldsymbol{G}_{11}\boldsymbol{\tau} - \boldsymbol{G}_{12}\boldsymbol{K}_\mu\boldsymbol{\zeta}_{\delta x} - \boldsymbol{G}_{11}\left[\boldsymbol{H}_{11}\dot{\boldsymbol{\theta}}_{\mathrm{r}} + \boldsymbol{H}_{12}\mu^2\dot{\boldsymbol{\zeta}}_{\delta x} \right] - \boldsymbol{G}_{12}\left[\boldsymbol{H}_{21}\dot{\boldsymbol{\theta}}_{\mathrm{r}} + \boldsymbol{H}_{22}\mu^2\dot{\boldsymbol{\zeta}}_{\delta x} \right] \tag{16}$$

$$\mu^2\ddot{\boldsymbol{\zeta}}_{\delta x} = \boldsymbol{G}_{21}\boldsymbol{\tau} - \boldsymbol{G}_{22}\boldsymbol{K}_\mu\boldsymbol{\zeta}_{\delta x} - \boldsymbol{G}_{21}\left[\boldsymbol{H}_{11}\dot{\boldsymbol{\theta}}_{\mathrm{r}} + \boldsymbol{H}_{12}\mu^2\dot{\boldsymbol{\zeta}}_{\delta x} \right] - \boldsymbol{G}_{22}\left[\boldsymbol{H}_{21}\dot{\boldsymbol{\theta}}_{\mathrm{r}} + \boldsymbol{H}_{22}\mu^2\dot{\boldsymbol{\zeta}}_{\delta x} \right] \tag{17}$$

In scenarios where $\mu \to 0$ is applicable, Eqs. (16) and (17) can be simplified to:

$$\ddot{\boldsymbol{\theta}}_{\mathrm{r}} = \left(\boldsymbol{G}_{11\,\mathrm{s}} - \boldsymbol{G}_{12\,\mathrm{s}}\boldsymbol{G}_{22\,\mathrm{s}}^{-1}\boldsymbol{G}_{21\,\mathrm{s}} \right)\left(-\boldsymbol{H}_{11\,\mathrm{s}}\dot{\boldsymbol{\theta}}_{\mathrm{r}} + \boldsymbol{\tau}_{\mathrm{s}} \right) \tag{18}$$

$$\boldsymbol{O} = \boldsymbol{G}_{21\,\mathrm{s}}\boldsymbol{\tau}_{\mathrm{s}} - \boldsymbol{G}_{22\,\mathrm{s}}\boldsymbol{K}_\mu\boldsymbol{\zeta}_{\delta 1\,\mathrm{s}} - \boldsymbol{G}_{21\,\mathrm{s}}\boldsymbol{H}_{11\,\mathrm{s}}\dot{\boldsymbol{\theta}}_{\mathrm{r}} - \boldsymbol{G}_{22\,\mathrm{s}}\boldsymbol{H}_{21\,\mathrm{s}}\dot{\boldsymbol{\theta}}_{\mathrm{r}} \tag{19}$$

In these expressions, the subscript signifies corresponding matrices or vectors when μ is equated to zero, leading to the derivation of the slow-varying (rigid) subsystem dynamic equation as shown in Eq. (20):

$$D_{\mathrm{s}}\ddot{\boldsymbol{\theta}}_{\mathrm{r}} + \boldsymbol{C}_{\mathrm{s}}\dot{\boldsymbol{\theta}}_{\mathrm{r}} = \boldsymbol{\tau}_{\mathrm{s}} \tag{20}$$

where, $\boldsymbol{D}_{\mathrm{s}} = \left(\boldsymbol{N}_{11\,\mathrm{s}} - \boldsymbol{N}_{12\,\mathrm{s}}\boldsymbol{N}_{22\,\mathrm{s}}^{-1}\boldsymbol{N}_{21\,\mathrm{s}} \right)^{-1}, \boldsymbol{C}_{\mathrm{s}} = \boldsymbol{C}_{11\,\mathrm{s}}$.

Defining the fast time scale $t_{\delta x}$ $(\mu t_{\delta x} = t - t_0)$ and the boundary layer correction terms $\boldsymbol{E}_1 = \boldsymbol{\zeta}_{\delta x} - \boldsymbol{\zeta}_{\delta x\,\mathrm{s}}$ and $\boldsymbol{E}_2 = \mu\dot{\boldsymbol{\zeta}}_{\delta x}$, Eq. (17) undergoes a transformation, leading to:

$$\mu\dot{\boldsymbol{E}}_2 = \boldsymbol{G}_{21}\boldsymbol{\tau} - \boldsymbol{G}_{22}\boldsymbol{K}_\mu\left(\boldsymbol{E}_1 + \boldsymbol{\zeta}_{\delta\mathrm{rs}} \right) - \boldsymbol{G}_{21}\left[\boldsymbol{H}_{11}\dot{\boldsymbol{\theta}}_{\mathrm{r}} + \boldsymbol{H}_{12}\mu\boldsymbol{E}_2 \right] - \boldsymbol{G}_{22}\left[\boldsymbol{H}_{21}\dot{\boldsymbol{\theta}}_{\mathrm{r}} + \boldsymbol{H}_{22}\mu\boldsymbol{E}_2 \right] \tag{21}$$

From this transformation, the following deductions are made:

$$\frac{\mathrm{d}\boldsymbol{E}_1}{\mathrm{d}t_{\delta x}} = \boldsymbol{E}_2 - \mu\dot{\boldsymbol{\zeta}}_{\delta x\,\mathrm{s}} \tag{22}$$

$$\frac{\mathrm{d}\boldsymbol{E}_2}{\mathrm{d}t_{\delta x}} = \boldsymbol{G}_{21}\boldsymbol{\tau} - \boldsymbol{G}_{22}\boldsymbol{K}_\mu\left(\boldsymbol{E}_1 + \boldsymbol{\zeta}_{\delta x\,\mathrm{s}} \right) - \boldsymbol{G}_{21}\left(\boldsymbol{H}_{11}\dot{\boldsymbol{\theta}}_{\mathrm{r}} + \boldsymbol{H}_{12}\mu\boldsymbol{E}_2 \right) - \boldsymbol{G}_{22}\left(\boldsymbol{H}_{21}\dot{\boldsymbol{\theta}}_{\mathrm{r}} + \boldsymbol{H}_{\delta\dot{\delta}}\mu\boldsymbol{E}_2 \right) \tag{23}$$

When controlling the attitude of the elastic base, the definition is as follows:

$$\boldsymbol{\tau}_{\delta x} = \boldsymbol{\tau} - \boldsymbol{\tau}_{\mathrm{s}} \tag{24}$$

By setting $\mu = 0$ and applying Eqs. (22) and (23), the fast-varying subsystem is effectively derived:

$$\frac{\mathrm{d}\boldsymbol{E}_1}{\mathrm{d}t_{\delta x}} = \boldsymbol{E}_2 \tag{25}$$

$$\frac{\mathrm{d}\boldsymbol{E}_2}{\mathrm{d}t_{\delta x}} = \boldsymbol{G}_{21\,\mathrm{s}}\boldsymbol{\tau}_{\delta x} - \boldsymbol{G}_{22\,\mathrm{s}}\boldsymbol{K}_\mu\boldsymbol{E}_1 \tag{26}$$

These equations are further elaborated upon as:

$$\dot{\boldsymbol{E}} = \boldsymbol{A}_{\delta x}\boldsymbol{E} + \boldsymbol{B}_{\delta x}\boldsymbol{\tau}_{\delta x} \tag{27}$$

where, $\boldsymbol{E} = \begin{bmatrix} \boldsymbol{E}_1^{\mathrm{T}}, \boldsymbol{E}_2^{\mathrm{T}} \end{bmatrix}^{\mathrm{T}}$, $\boldsymbol{A}_{\delta x} = \begin{bmatrix} \boldsymbol{0}_{n_i n \times n_i n} & \boldsymbol{I}_{n_i n \times n_i n} \\ -\boldsymbol{N}_{22\,\mathrm{s}} \boldsymbol{K}_\mu & \boldsymbol{0}_{n_i n \times n_i n} \end{bmatrix}$, and $\boldsymbol{B}_{\delta x} = \begin{bmatrix} \boldsymbol{0}_{n_i n \times (n+1)} \\ \boldsymbol{N}_{21\,\mathrm{s}} \end{bmatrix}$, $\boldsymbol{\tau}_{\delta x}$ represents the control schemes deployed within the fast-varying subsystem.

The control objective for the fully-flexible arm space robot system, under the influence of an elastic base, is meticulously formulated. The aim is to design precise control inputs that facilitate the accurate tracking of desired trajectories by the robotic arm's joints, alongside controlling the vibration of the partially decoupled system as represented in Eq. (12). The culmination of this objective is a comprehensive control scheme for the fully-flexible arm space robot. This scheme synergistically combines the control strategies $\boldsymbol{\tau}_{\mathrm{s}}$ and $\boldsymbol{\tau}_{\delta x}$ for both the slow-varying and fast-varying subsystems. The application of the singular perturbation reduction method concurrently stabilizes the trajectory tracking of joint hinges and attenuates system vibrations. The total control torque expression, tailored for systems with controlled base attitudes, is captured in:

$$\boldsymbol{\tau} = \boldsymbol{\tau}_{\mathrm{s}} + \boldsymbol{\tau}_{\delta x} \tag{28}$$

4 Control Scheme Design

In alignment with the findings from Section 3, the fully-flexible arm space robot system, influenced by an elastic base and analyzed through singular perturbation theory, is segregated into two subsystems: a slow-varying subsystem, which encapsulates joint rigid motion, and a fast-varying subsystem, which accounts for vibrations of the elastic base and flexible arms. These subsystems, being temporally independent, allow for the formulation of distinct control schemes, which are then amalgamated to establish an integrated control framework for the entire system.

4.1 Control Scheme Design for the Slow-Varying Subsystem

In real-world space robot systems, perturbations in system parameters due to measurement errors, environmental fluctuations, and load variations are a given. Consequently, the parameter matrix, as delineated in Eq. (20), is characterized thus:

$$\begin{cases} D_{\mathrm{s}} = D_{\mathrm{s}0} + \Delta D_{\mathrm{s}} \\ \boldsymbol{C}_{\mathrm{s}} = \boldsymbol{C}_{\mathrm{s}0} + \Delta \boldsymbol{C}_{\mathrm{s}} \end{cases} \tag{29}$$

where, $\boldsymbol{D}_{\mathrm{s}0}$ and $\boldsymbol{C}_{\mathrm{s}0}$ signify the nominal components of the parameters, and $\Delta \boldsymbol{D}_{\mathrm{s}}$ and $\Delta \boldsymbol{C}_{\mathrm{s}}$ represent the uncertainty aspects of parameter perturbations.

Setting $\boldsymbol{x}_1 = \boldsymbol{\theta}_{\mathrm{r}}$ and $\boldsymbol{x}_2 = \dot{\boldsymbol{\theta}}_{\mathrm{r}}$, with $\boldsymbol{x} = \begin{bmatrix} \boldsymbol{x}_1^{\mathrm{T}}, \boldsymbol{x}_2^{\mathrm{T}} \end{bmatrix}^{\mathrm{T}}$, and considering a specific desired trajectory $\boldsymbol{x}_{\mathrm{d}} = [q_{\mathrm{d}0}, q_{\mathrm{d}1}, q_{\mathrm{d}2}, \cdots, q_{\mathrm{d}n}]^{\mathrm{T}}$, Eq. (20) can be reformulated as:

$$\begin{cases} \dot{x}_1 = x_2 \\ \dot{x}_2 = f(x) + g(x)\tau_{\mathrm{s}} + \Delta \\ y = \beta \boldsymbol{x} \end{cases} \tag{30}$$

where, $\boldsymbol{f}(\boldsymbol{x}) = -\boldsymbol{D}_{\mathrm{s}0}^{-1} \boldsymbol{C}_{\mathrm{s}0} \dot{\boldsymbol{\theta}}_{\mathrm{r}}, \boldsymbol{g}(\boldsymbol{x}) = \boldsymbol{D}_{\mathrm{s}0}^{-1}$, $\beta = [1, 0]$, and $\Delta = -\boldsymbol{D}_{\mathrm{s}0}^{-1} \left(\Delta \boldsymbol{D}_{\mathrm{s}} \ddot{\boldsymbol{\theta}}_{\mathrm{r}} + \Delta \boldsymbol{C}_{\mathrm{s}} \dot{\boldsymbol{\theta}}_{\mathrm{r}} \right)$ quantifies the uncertainty within the parameters of the slow-varying subsystem.

The primary goal is to address the joint trajectory tracking challenge within the system, where only joint positions are measurable, and joint velocities are not required to be measured. Utilizing the dynamics equation of the slow-varying subsystem from Eq. (20), a design approach involving a Luenberger nonlinear observer [23, 24] is proposed. This observer aims to provide estimates of the arm joint angular velocities, as described in:

$$\begin{cases} \dot{\hat{x}}_1 = \hat{x}_2 + \boldsymbol{L}_1 \left(\boldsymbol{x}_1 - \hat{\boldsymbol{x}}_1 \right) \\ \dot{\hat{x}}_2 = \boldsymbol{f}(\hat{\boldsymbol{x}}) + \boldsymbol{g}(\hat{\boldsymbol{x}})\tau_{\mathrm{s}} + \Delta + \boldsymbol{L}_2 \left(\boldsymbol{x}_1 - \hat{\boldsymbol{x}}_1 \right) \\ \hat{y} = \beta \hat{\boldsymbol{x}} \end{cases} \tag{31}$$

An RBF neural network is applied within the observer Eq. (31) to estimate the system parameter uncertainties Δ. The unknown continuous nonlinear function is represented through a neural network composed of ideal weights $\boldsymbol{W}$ and a sufficient number of basis functions $\xi(x)$:

$$\Delta = \boldsymbol{W}^* \boldsymbol{\xi}(x) + \varepsilon(x) \tag{32}$$

where, $\varepsilon(x)$ symbolizes the neural network approximation error.

Assuming the ideal weights $\boldsymbol{W}^*$ are bounded, i.e. $\|\boldsymbol{W}^*\|_{\mathrm{F}} \leq \boldsymbol{W}_{\mathrm{M}}$, an adaptive law for neural network weights is defined:

$$\dot{\hat{\boldsymbol{W}}} = \boldsymbol{\Xi} \left(\boldsymbol{\xi} z^{\mathrm{T}} - \sigma \hat{\boldsymbol{W}} \right) \tag{33}$$

where, $\boldsymbol{\Xi}$ is a reversible and positive matrix, $\sigma > 0$ serves as a modification factor, $\hat{\boldsymbol{W}}$ represents the estimated value of the ideal weight matrix $\boldsymbol{W}^*$ of the RBF neural network, and $\tilde{\boldsymbol{W}} = \hat{\boldsymbol{W}} - \boldsymbol{W}^*$ is the weight estimation error.

A Gaussian function is selected as the radial basis function for the neural network:

$$\boldsymbol{\xi} = \exp\left(-\frac{\|x - c\|^2}{2b^2}\right) \tag{34}$$

where, c and b, respectively, are the center vector and width of the basis.

Upon defining $\tilde{\boldsymbol{z}}_1 = \boldsymbol{x}_1 - \hat{\boldsymbol{x}}_1$ and $\tilde{\boldsymbol{z}}_2 = \boldsymbol{x}_2 - \hat{\boldsymbol{x}}_2$, the subsequent formulation is derived:

$$\begin{cases} \dot{\tilde{z}}_1 = \boldsymbol{x}_2 - \hat{\boldsymbol{x}}_2 - \boldsymbol{L}_1 \left(\boldsymbol{x}_1 - \hat{\boldsymbol{x}}_1\right) \\ \dot{\tilde{z}}_2 = \boldsymbol{f}(\boldsymbol{x}) - \boldsymbol{f}(\hat{\boldsymbol{x}}) + [\boldsymbol{g}(\boldsymbol{x}) - \boldsymbol{g}(\hat{\boldsymbol{x}})]\boldsymbol{\tau}_\mathrm{s} - \boldsymbol{L}_2 \left(\boldsymbol{x}_1 - \hat{\boldsymbol{x}}_1\right) \end{cases} \tag{35}$$

where, $\boldsymbol{L} = [\boldsymbol{L}_1, \boldsymbol{L}_2]^\mathrm{T}$ represents the gain of the Luenberger observer, a parameter that can be strategically configured in accordance with Luenberger observer theory.

The following definitions are set forth:

$$f = \begin{bmatrix} f_1 \\ f_2 \end{bmatrix} = \begin{bmatrix} x_2 - \hat{x}_2 \\ f(x) - f(\hat{x}) \end{bmatrix} \tag{36}$$

$$g = \begin{bmatrix} 0 \\ g(x) - g(\hat{x}) \end{bmatrix} \tag{37}$$

A selection of $\boldsymbol{L} = [\boldsymbol{L}_1, \boldsymbol{L}_2]^\mathrm{T}$ is made such that $\left.\frac{\partial \boldsymbol{f}}{\partial \boldsymbol{x}}\right|_{\boldsymbol{x}=0} - \boldsymbol{L} \cdot \left.\frac{\partial \boldsymbol{y}}{\partial \boldsymbol{x}}\right|_{\boldsymbol{x}=0}$ is established as a Hurwitz matrix. $\boldsymbol{L}_1 = \mathrm{diag}\left(L_{11}, L_{12}, \cdots, L_{1n}\right)$ and $\boldsymbol{L}_2 = \mathrm{diag}\left(L_{21}, L_{22}, \cdots, L_{2n}\right)$ are identified as the gain matrices pertinent to the Luenberger observer.

When $\boldsymbol{f}' = \begin{bmatrix} \boldsymbol{x}_2 \\ \boldsymbol{f}(\boldsymbol{x}) \end{bmatrix}$ and $\boldsymbol{g}' = \begin{bmatrix} \boldsymbol{0} \\ \boldsymbol{g}(\boldsymbol{x}) \end{bmatrix}$ are stipulated, leading to the linearization of the formula, the ensuing relationship is:

$$\dot{\tilde{z}}_i = A\tilde{\boldsymbol{z}}_i + B\boldsymbol{\tau}_\mathrm{s} - \boldsymbol{K}\tilde{\boldsymbol{z}}_1 = A\tilde{\boldsymbol{z}}_i + B\boldsymbol{\tau}_\mathrm{s} - \boldsymbol{L}\beta\tilde{\boldsymbol{z}}_1, i = 1, 2 \tag{38}$$

Applying the principles of Luenberger observer theory and selecting $\boldsymbol{L} = [\boldsymbol{L}_1, \boldsymbol{L}_2]^\mathrm{T}$ to ensure that $A - \boldsymbol{L}\beta$ is a Hurwitz matrix, the designed Luenberger observer's convergence is validated. The consequent equation is:

$$A = \left.\frac{\partial \boldsymbol{f}'}{\partial \boldsymbol{x}}\right|_{\boldsymbol{x}=0} = \begin{bmatrix} \frac{\partial \boldsymbol{f}_1'}{\partial \boldsymbol{x}_1} & \frac{\partial \boldsymbol{f}_1'}{\partial \boldsymbol{x}_2} \\ \frac{\partial \boldsymbol{f}_2'}{\partial \boldsymbol{x}_1} & \frac{\partial \boldsymbol{f}_2'}{\partial \boldsymbol{x}_2} \end{bmatrix}, \quad \boldsymbol{L}\beta = \boldsymbol{L} \cdot \left.\frac{\partial \boldsymbol{y}}{\partial \boldsymbol{x}}\right|_{\boldsymbol{x}=0} = [\boldsymbol{L}_1, \boldsymbol{L}_2]^\mathrm{T} [\boldsymbol{I}, \boldsymbol{0}] = \begin{bmatrix} \boldsymbol{L}_1 & \boldsymbol{0} \\ \boldsymbol{L}_2 & \boldsymbol{0} \end{bmatrix}.$$

Integrating the various inertial parameters of the fully-flexible arm space robot under the elastic base influence, the eigenvalues of $A - \boldsymbol{L}\beta$ are positioned in the left half of the plane s, resulting in the determination of $\boldsymbol{L}_1$ and $\boldsymbol{L}_2$ values.

A Proportional-Derivative (PD) control scheme is devised for tracking the desired joint position, as delineated in:

$$\tau_\mathrm{s} = \boldsymbol{K}_\mathrm{p}e + \boldsymbol{K}_\mathrm{d}\dot{e} + D_\mathrm{s0}\ddot{x}_\mathrm{d} + \boldsymbol{C}_\mathrm{s0}\dot{x}_\mathrm{d} \tag{39}$$

where, $\boldsymbol{K}_\mathrm{p}$ symbolizes the proportional feedback coefficient, and $\boldsymbol{K}_\mathrm{d}$ the velocity feedback coefficient. $\boldsymbol{e} = \hat{\boldsymbol{x}}_1 - \boldsymbol{x}_\mathrm{d}$ denotes the estimated joint angle error, while $\dot{\boldsymbol{e}} = \hat{\boldsymbol{x}}_2 - \dot{\boldsymbol{x}}_\mathrm{d}$ represents the estimated joint angular velocity error. Through appropriate adjustments of $\boldsymbol{K}_\mathrm{p}$ and $\boldsymbol{K}_\mathrm{d}$, the motion tracking error is engineered to converge to zero.

4.2 Control Scheme Design for the Fast-Varying Subsystem

For the fast-varying subsystem, as explicated in Eq. (27), the adoption of a Linear Quadratic Regulator (LQR) control scheme is proposed to regulate the system states $\boldsymbol{E}$ effectively. This approach is aimed at reducing these states to zero, actively mitigating the vibrations instigated by the base and arm rods. To facilitate this, a system performance index function is established, as follows:

$$J_{\delta x} = \frac{1}{2} \int_0^\infty \left(\boldsymbol{\tau}_{\delta x}^\mathrm{T} \boldsymbol{R}_{\delta x} \boldsymbol{\tau}_{\delta x} + \boldsymbol{E}^\mathrm{T} \boldsymbol{Q}_{\delta x} \boldsymbol{E}\right) \mathrm{d}t \tag{40}$$

where, $\boldsymbol{R}_{\delta x}$ and $\boldsymbol{Q}_{\delta x}$ serve as the weighting matrices for the control vector $\boldsymbol{\tau}_{\delta x}$ and the state vector $\boldsymbol{E}$, respectively.

The unique solution to the Riccati equation, essential for the optimal functioning of this subsystem, is identified as $\boldsymbol{P}_{\delta x}$:

$$\boldsymbol{P}_{\delta x}\boldsymbol{A}_{\delta x} + \boldsymbol{A}_{\delta x}^{\mathrm{T}}\boldsymbol{P}_{\delta x} - \boldsymbol{P}_{\delta x}\boldsymbol{B}_{\delta x}\boldsymbol{R}_{\delta x}^{-1}\boldsymbol{B}_{\delta x}^{\mathrm{T}}\boldsymbol{P}_{\delta x} + \boldsymbol{Q}_{\delta x} = 0 \tag{41}$$

Subsequently, the optimal control scheme for the fast-varying subsystem is articulated:

$$\boldsymbol{\tau}_{\delta x} = -\boldsymbol{R}_{\delta x}^{-1}\boldsymbol{B}_{\delta x}^{\mathrm{T}}\boldsymbol{P}_{\delta x}\boldsymbol{E} \tag{42}$$

5 Numerical Simulation Example

A dynamic numerical simulation was conducted on a space robotic arm system featuring two flexible arms and influenced by an elastic base in plane motion. The simulation spanned a total duration of t=15s. Parameters of this two-flexible-rod space robotic arm system, under the elastic base influence, are detailed in Table 1.

In this simulation, the number of flexible arms was set as n=2. The estimated values for the bending interface modulus were selected as $E\hat{I}_1 = 0.5EI_1$ and $E\hat{I}_2 = 0.5EI_2$. Other computational parameters in the simulation include: a modification factor $\sigma = 0.1$, a basis function width $b = 2$, uniformly distributed initial node centers c within $[-2,+2]$, observation gains $\boldsymbol{L}_1 = \mathrm{diag}[5,5,5]$ and $\boldsymbol{L}_2 = \mathrm{diag}[4,4,4]$, a proportional feedback coefficient $\boldsymbol{K}_{\mathrm{p}} = \mathrm{diag}[50,50,50]$, a velocity feedback coefficient $\boldsymbol{K}_{\mathrm{d}} = \mathrm{diag}[64,64,64]$, and a reversible positive gain matrix $\boldsymbol{E} = \mathrm{diag}[0.5,0.5,0.5,0.5,0.5,0.5]$, $\boldsymbol{R} = \mathrm{diag}[1,1,1]$, and $\boldsymbol{Q} = 100 \cdot \mathrm{diag}[1,1,1,1,1,1,1,1,1,1]$.

Table 1. System parameters of the space robot with elastic base and flexible arms

Parameters	Values
Base inertial parameters	$m_0 = 200$ kg, $l_0 = 1.5$ m, $\quad j_0 = 70$ kg $\cdot$ m^2
Arm rod B_1	$l_1 = 3$ m, $\rho_1 = 1.1$ kg/m, $EI_1 = 50$ N $\cdot$ m^2
Arm rod B_2	$l_2 = 3$ m, $\quad \rho_2 = 1.1$ kg/m, $EI_2 = 50$ N $\cdot$ m^2
Base	$\boldsymbol{K}_x = 50$ N/m

The desired motion trajectories for the system's carrier and each joint angle were established as:

$$q_{\mathrm{d}0} = \frac{\pi}{2}\mathrm{rad}, q_{\mathrm{d}1} = \frac{7\pi}{16}\mathrm{rad}, q_{\mathrm{d}2} = \frac{3\pi}{8}\mathrm{rad},$$

The initial motion position of the system was set as:

$$q_0(0) = 1.68\mathrm{rad}, q_1(0) = 1.25\mathrm{rad}, q_2(0) = 1.25\mathrm{rad}, \boldsymbol{x}'(0) = 0 \text{ m}, \delta_{11}(0) = \delta_{12}(0) = 0 \text{ m}, \delta_{21}(0) = \delta_{22}(0) = 0 \text{ m}.$$
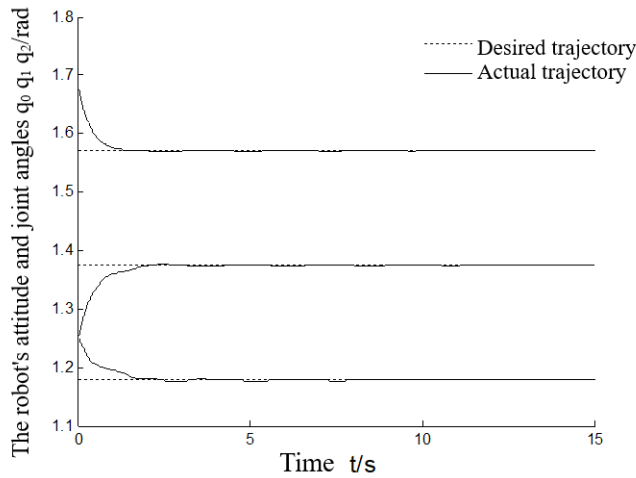

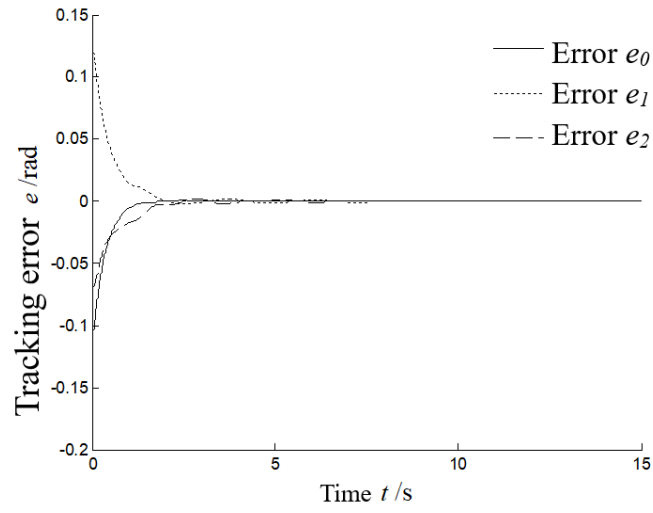**Figure 2.** Position tracking of the elastic base's attitude and joint angles

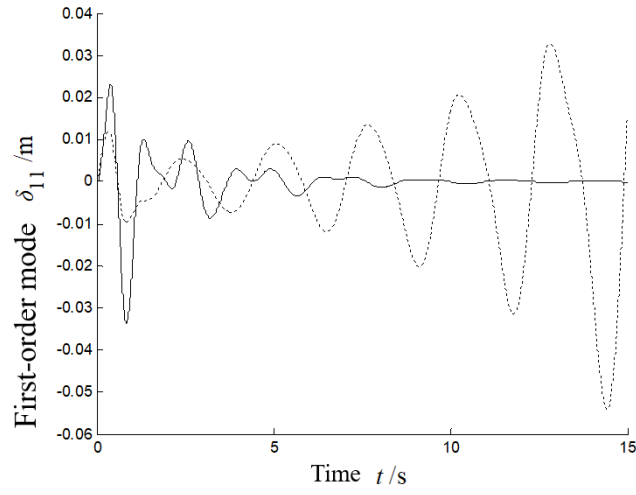**Figure 3.** Position tracking errors of the elastic base's attitude and joint angless

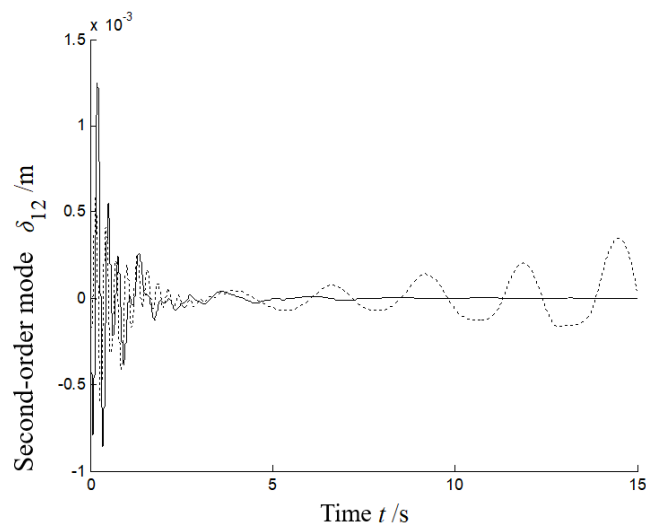**Figure 4.** First-order vibration modal coordinates of the flexible arm rod B_1

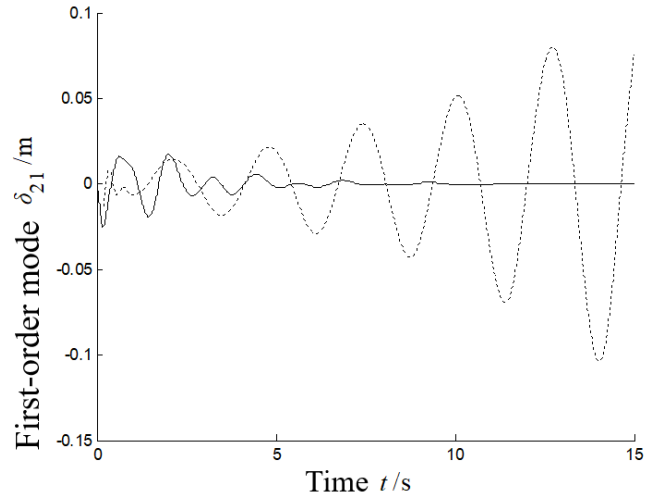**Figure 5.** Second-order vibration modal coordinates of the flexible arm rod B_1

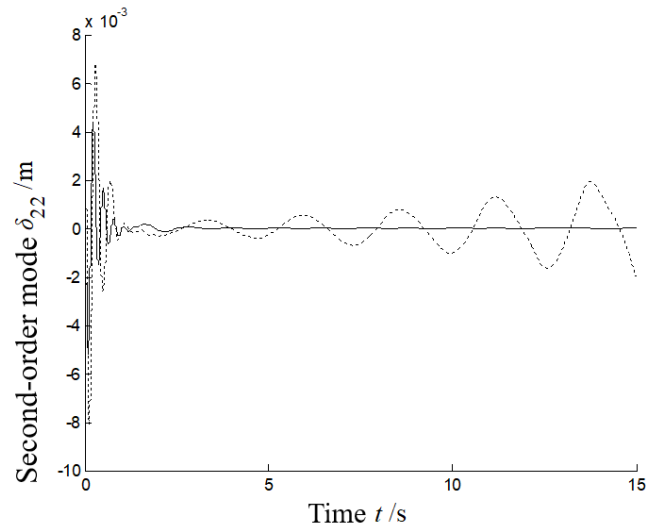**Figure 6.** First-order vibration modal coordinates of the flexible arm rod B_2

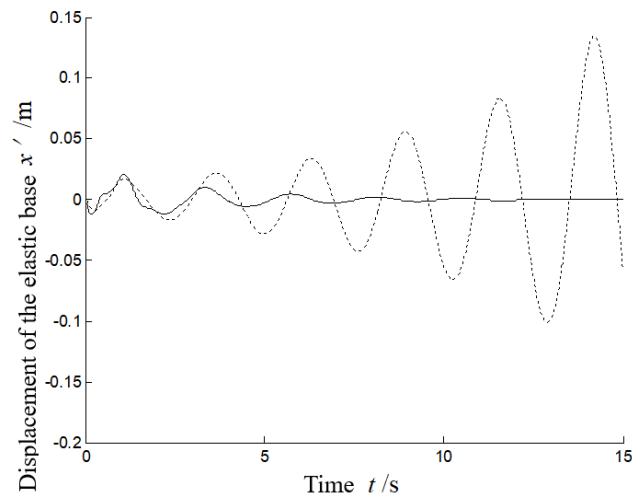**Figure 7.** Second-order vibration modal coordinates of the flexible arm rod B_2

Figure 8. Displacement of the elastic base

The simulation results, illustrated in Figures 2 to 8, encompass various aspects of system behavior. Figure 2 displays the position tracking of the elastic base's attitude angle and the arm rod joint angles, while Figure 3 shows the tracking errors of these angles. Figures 4 and 6 present the first-order vibration modal coordinates of the flexible arms B_1 and B_2, and Figures 5 and 7 depict the second-order vibration modal coordinates. Figure 8 provides a visualization of the displacement of the elastic base. Notably, from Figures 4 to 8, it is observed that the activation of the fast-varying subsystem control scheme, indicated by solid lines, compared to its deactivation, shown by dashed lines, not only rapidly converges the system's tracking error to zero but also effectively suppresses the flexible vibrations of the system. This result underscores the precision and stability of the system's trajectory tracking within the joint space.

6 Conclusion

In this study, an established model of a fully-flexible arm space robot system, operating under the influence of an elastic base, was meticulously examined. Challenges such as the vibrations of the elastic base and flexible arms, parameter uncertainties, and the non-necessity of measuring joint velocities were addressed through several strategic steps. Initially, the system's dynamics model underwent a decoupling process using a dual-scale singular perturbation method, resulting in the division of the system into two subsystems: a slow-varying subsystem, characterizing joint rigid motion, and a fast-varying subsystem, focusing on the vibrations of the elastic base and flexible arms. Subsequently, a composite control scheme was developed. This scheme combined a PD control, based on the Luenberger observer for the slow-varying subsystem, with a linear optimal control strategy for the fast-varying subsystem.

Numerical simulations were conducted to evaluate the effectiveness of the proposed composite control scheme. The results demonstrated that the scheme was capable of precisely controlling the rigid motion of the robotic arm's joints while simultaneously and effectively suppressing the vibrations of both the base and arm rods. A significant advantage of this approach was the utilization of the Luenberger observer for estimating joint velocities. This method obviated the need for direct measurement and feedback of velocity information pertaining to the system's base attitude angle and arm joint angles, thereby offering potential cost savings in the operation of space equipment.

Data Availability

The data used to support the findings of this study are available from the corresponding author upon request.

Conflicts of Interest

The authors declare that they have no conflicts of interest.

References

[1] T. Rybus, M. Wojtunik, and F. L. Basmadji, "Optimal collision-free path planning of a free-floating space robot using spline-based trajectories," *Acta Astronaut.*, vol. 190, pp. 395–408, 2022. https://doi.org/10.1016/j.actaastro.2021.10.012

[2] T. Rybus, "Obstacle avoidance in space robotics: Review of major challenges and proposed solutions," *Prog. Aerosp. Sci.*, vol. 101, pp. 31–48, 2018. https://doi.org/10.1016/j.paerosci.2018.07.001

[3] K. Facciol, T. Braithwaite, L. Lefebvre, and E. Tabarah, "Canada and the international space station program: Overview and status," in *54th International Astronautical Congress of the International Astronautical Federation, the International Academy of Astronautics, and the International Institute of Space Law, Bremen, Germany*, 2019. https://doi.org/10.2514/6.IAC-03-T.1.04

[4] G. Misra and X. Bai, "Optimal path planning for free-flying space manipulators via sequential convex programming," *J. Guid. Control. Dyn.*, vol. 40, no. 11, pp. 3019–3026, 2017. https://doi.org/10.2514/1.G002487

[5] J. Ratajczak and K. Tchoń, "Normal forms and singularities of non-holonomic robotic systems: A study of free-floating space robots," *Syst. Control Lett.*, vol. 138, p. 104661, 2020. https://doi.org/10.1016/j.sysconle.2020.104661

[6] R. Boumans and C. Heemskerk, "The European robotic arm for the international space station," *Robot. Auton. Syst.*, vol. 23, no. 1-2, pp. 17–27, 1998. https://doi.org/10.1016/S0921-8890(97)00054-7

[7] A. Flores-Abad, O. Ma, K. Pham, and S. Ulrich, "A review of space robotics technologies for on-orbit servicing," *Prog. Aerosp. Sci.*, vol. 68, pp. 1–26, 2014. https://doi.org/10.1016/j.paerosci.2014.03.002

[8] H. Delavari, P. Lanusse, and J. Sabatier, "Fractional order controller design for a flexible link manipulator robot," *Asian J. Control*, vol. 15, no. 3, pp. 783–795, 2013. https://doi.org/10.1002/asjc.677

[9] M. Sabatini, P. Gasbarri, R. Monti, and G. B. Palmerini, "Vibration control of a flexible space manipulator during on orbit operations," *Acta Astronaut.*, vol. 73, pp. 109–121, 2012. https://doi.org/10.1016/j.actaastro.2011.11.012

[10] D. Huang and L. Chen, "Inverse kinematic control of free-floating space robot system based on a mutual mapping neural network," in *2008 7th World Congress on Intelligent Control and Automation, Chongqing, China*, 2008, pp. 8666–8670. https://doi.org/10.1109/WCICA.2008.4594293

[11] L. Zhang and L. Chen, "Fuzzy robust $h\infty$ control and flexible vibration optimal control for free-floating flexible space manipulator," *China Mech. Eng.*, vol. 27, no. 18, p. 2447, 2016. http://www.cmemo.org.cn/EN/Y2016/V27/I18/2447

[12] C. Jing and C. Li, "Mechanical analysis and calm control of dual-arm space robot for capturing a satellite," *Chin. J. Theor. Appl. Mech.*, vol. 48, no. 4, pp. 832–842, 2016. https://doi.org/10.6052/0459-1879-16-156

[13] H. Halalchi, E. Laroche, and G. I. Bara, "Flexible-link robot control using a linear parameter varying systems methodology," *Int. J. Adv. Robot. Syst.*, vol. 11, no. 3, p. 46, 2014. https://doi.org/10.5772/57325

[14] A. Shawky, D. Zydek, Y. Z. Elhalwagy, and A. Ordys, "Modeling and nonlinear control of a flexible-link manipulator," *Appl. Math. Model.*, vol. 37, no. 23, pp. 9591–9602, 2013. https://doi.org/10.1016/j.apm.2013.05.003

[15] K. Senda and Y. Murotsu, "Methodology for control of a space robot with flexible links," *IEE Proc.-Control Theory Appl.*, vol. 147, no. 6, pp. 562–568, 2000. https://doi.org/10.1049/ip-cta:20000870

[16] S. M. Joshi, G. Arunkumar, and T. C. Manjunath, "Control of n-link flexible robotic manipulators in 3D Euclidean space using PID, POF, FOS & DSMC strategies," *Int. J. Grid Distrib. Comput.*, 2019. http://hdl.handle.net/10603/452458

[17] L. Evans, "Canadian space robotics on board the international space station," in *2005 CCToMM Symposium on Mechanisms, Machines, and Mechatronics, Montreal, Canada*, 2005, pp. 26–27.

[18] W. Chen, "Dynamic modeling of multi-link flexible robotic manipulators," *Comput. Struct.*, vol. 79, no. 2, pp. 183–195, 2001. https://doi.org/10.1016/S0045-7949(00)00129-2

[19] R. V. Patel, M. Toda, and B. Sridhar, "Robustness of linear quadratic state feedback designs in the presence of system uncertainty," *IEEE Trans. Autom. Control*, vol. 22, no. 6, pp. 945–949, 1977. https://doi.org/10.1109/TAC.1977.1101658

[20] S. Dubowsky and E. Papadopoulos, "The kinematics, dynamics, and control of free-flying and free-floating space robotic systems," *IEEE Trans. Robot. Autom.*, vol. 9, no. 5, pp. 531–543, 1993. https://doi.org/10.1109/70.258046

[21] A. Seddaoui, C. M. Saaj, and M. H. Nair, "Modeling a controlled-floating space robot for in-space services: A beginner's tutorial," *Front. Robot. AI*, vol. 8, p. 725333, 2021. https://doi.org/10.3389/frobt.2021.725333

[22] K. Nanos and E. G. Papadopoulos, "On the dynamics and control of free-floating space manipulator systems in the presence of angular momentum," *Front. Robot. AI*, vol. 4, p. 26, 2017. https://doi.org/10.3389/frobt.2017.00026

[23] F. J. Bejarano and M. Mera, "Robust luenberger-like observer for control of linear switched systems under arbitrary unknown switched function," *Asian J. Control*, vol. 23, no. 6, pp. 2527–2536, 2021. https://doi.org/10.1002/asjc.2406

[24] M. Hammouche, A. Mohand-Ousaid, P. Lutz, and M. Rakotondrabe, "Robust interval luenberger observer-based state feedback control: Application to a multi-DOF micropositioner," *IEEE Trans. Control Syst. Technol.*, vol. 27, no. 6, pp. 2672–2679, 2018. https://doi.org/10.1109/TCST.2018.2865767